A Force Reflected Exoskeleton-Type Masterarm for Human–Robot Interaction

Yoon Sang Kim, *Member, IEEE*, Jangwook Lee, Sooyong Lee, *Member, IEEE*, and Munsang Kim, *Member, IEEE*

***Abstract*—Two human–robot interactions, including a haptic interaction and a teleoperated interaction, are explored in this paper with a new exoskeleton-type masterarm, in which the electric brakes with the torque sensor beams are used for force reflection. In the haptic interaction with virtual environment, the masterarm is used as a haptic device and tested to examine how the resistant torque of the electric brake for the force reflection is implemented in contact regime prior to conducting the teleoperated interaction. Two types of virtual environments, a rigid wall with high stiffness (hard contact with 10 [KN/m]) and a soft wall with low stiffness (soft contact with 0.1 [N/m]), are integrated with the masterarm for the haptic interaction. In hard contact, large force is fed back to the human operator, and makes the human operator hardly move. The electric brake with the torque sensor beam can detect the torque and its direction so that it allows free motion as well as contact motion by releasing or holding the movement of the operator. The experimental results show how the electric brake is switched from contact to free regime to allow the operator to move freely, especially when the operator intends to move toward the free regime in contact. In soft contact, the force applied to the human operator can be increased or decreased proportionally to the torque amount sensed by the torque sensor beam, thus the operator can feel the contact force proportional to the amount of the deformation during the contact. Finally, the masterarm is integrated with the humanoid robot, CENTAUR developed at Korea Institute of Science and Technology to conduct a pick-and-place task through the teleoperated interaction. It is examined that the CENTAUR as a slave robot can follow the movement of the operator.**

***Index Terms*—Exoskeleton masterarm, force reflection, haptic interaction, human–robot interaction, teleoperated interaction.**

I. Introduction

ROBOTS do not have sufficient capabilities to perform complex tasks unless it is completely autonomous. Numerous studies have been done over the years on the human–robot interaction through teleoperated interaction (teleoperation) to make it possible for a supervisor to command the robot from a remote site monitoring the interaction of the robot with its environments [1]. In addition to teaching capability, the human operator can have more realistic interaction with the environment by providing feedback. There is an obvious need to use feedback from widely differing sensors in order to properly monitor various aspects of the task, especially for complex tasks. In human–robot interaction for object manipulation, force and vision feedback are the most important sensing modes. Vision is useful for aligning objects, while force ensures reasonable contact forces to be maintained as parts mating occurs.

In force-reflecting master-slave systems, forces are measured at the slave and transmitted to the master system. Since the pioneering work of Goertz [2], a number of similar systems and schemes have been proposed. In recent years, the feedback of tactile and kinesthetic sensory input have been suggested for the application through haptic interaction in virtual reality technology [3]–[5]. The interest in force-feedback systems for virtual reality applications has led to the development of many systems, ranging from force-reflecting mouses (joysticks) to whole force feedback arm-exoskeletons [4]–[12].

Most of the exoskeleton-type masterarms have a kinematic design similar to that of the slave arm, with actuators, usually electric motors, thus making the masterarm bulky and heavy. Lee *et al.* [13] introduced the exoskeleton-type masterarm with pneumatic actuators, which is very light and compact, but requires a compressed air supply to implement force feedback. Teleoperation with motion capturing devices was introduced [14], which generates the slave robot's motion command from the partitioned inverse kinematics, showing that the masterarm's kinematic structure does not have to be the same as the slave robot's. The distributed controller architecture was introduced [15], which makes possible the efficient allocation of controlling and sensing communication tasks as well as simple wiring for better implementation and maintenance. In the latest work [16], a new exoskeleton-type masterarm for force reflection was proposed based on the previous efforts. To provide electric brakes as actuators for force reflection with the force functionality to sense the torque, as well as its direction, the torque sensor beam was designed and added to each active joint module. By detecting the torque as well as its direction applied by the human operator, it allowed the electric brake to be used as an actuator for the force reflection. The use of electric brakes as actuators for the force reflection made the masterarm light and compact, less than 3 kg in weight felt by the human operator on each arm.

In this paper, our work is extended to human–robot interaction by using the proposed masterarm. In Sections II–V, our previous efforts on the development of the proposed masterarm are reviewed. A kinematic design and analysis for the proposed masteram is reviewed in Section II. Calibration algorithm to

Manuscript received May 28, 2003; revised March 4, 2004. This work was supported by the Korean Ministry of Science and Technology. This paper was recommended by Associate Editor A. Ollero.

Y. S. Kim is with the Interaction Laboratory, Samsung Advanced Institute of Technology (SAIT), Suwon 440-600, Korea (e-mail: yoonsang.kim@samsung.com).

J. Lee is with the Telecom Billing System, SK C&C, Seoul 100-753, Korea (e-mail: tante@skcc.com).

S. Lee is with the Department of Mechanical and System Design Engineering, Hongik University, Seoul 121-791, Korea (e-mail: sooyong@hongik.ac.kr).

M. Kim is with the Intelligent Robot–The Frontier 21 Program, Korea Institute of Science and Technology (KIST), Seoul 136-791, Korea (e-mail: munsang@kist.re.kr).

Digital Object Identifier 10.1109/TSMCA.2004.832836

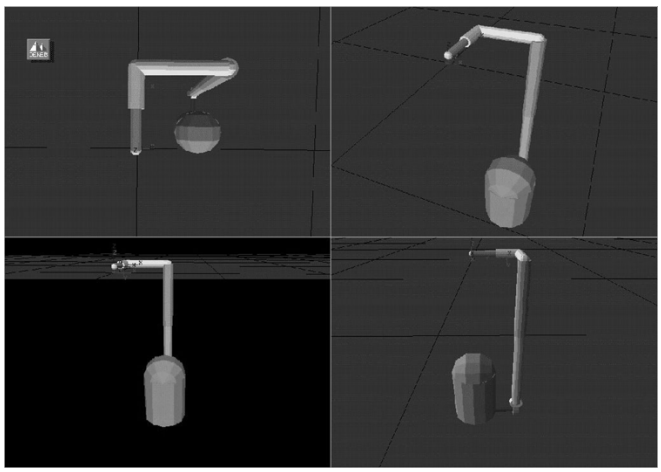

Fig. 1. Design simulation for the upper arm.

compensate the variation of the kinematic parameters is described in Section III. Each active joint module of the proposed masterarm for force feedback is tested in Section IV, and the two experimental results follow. In Section V, two human–robot interactions with the masterarm, including a haptic interaction and a teleoperated interaction, are explored in which electric brakes are used as actuators for force reflection with the torque sensor beam. In the haptic interaction, the masterarm is used as a haptic device, while it is used as a motion commander in the teleoperated interaction. In the haptic interaction with virtual environment, the masterarm as a haptic device is tested for force reflection in the contact regime prior to conducting the teleoperated interaction. Two types of virtual environments, a rigid wall with high stiffness (hard contact with 10 [KN/m]) and a soft wall with low stiffness (soft contact with 0.1 [N/m]), are integrated with the masterarm for the haptic interaction. The masterarm is integrated with the humanoid robot, CENTAUR developed at the Korea Institute of Science and Technology (KIST). The postures and motions of the robot and the operator are measured and compared to examine that the humanoid robot as a slave can follow the movement of the operator. Two mastergloves and a Fastrak sensor are added to the overall system to generate the motions of the CENTAUR's waist, neck, and hands (fingers).

II. Kinematic Design and Analysis

The following design goals are taken into consideration in designing the proposed masterarm with a serial link mechanism.

1) The masterarm's joint angle is to be measured in joint coordinates, rather than by using position/orientation sensors in Cartesian coordinates, thus simplifying the forward kinematics of the masterarm.
2) Movement of the human operator who wears the masterarm should not be constrained by the joint limit or collision with the links of the masterarm.
3) To achieve the maximum coverage of the human operator's movement, additional redundant joints may be added, if necessary.
4) Even with redundant joints, fewer numbers of joints with encoders and actuators are preferred for implementation.
5) It is preferred not to have any singular configuration.

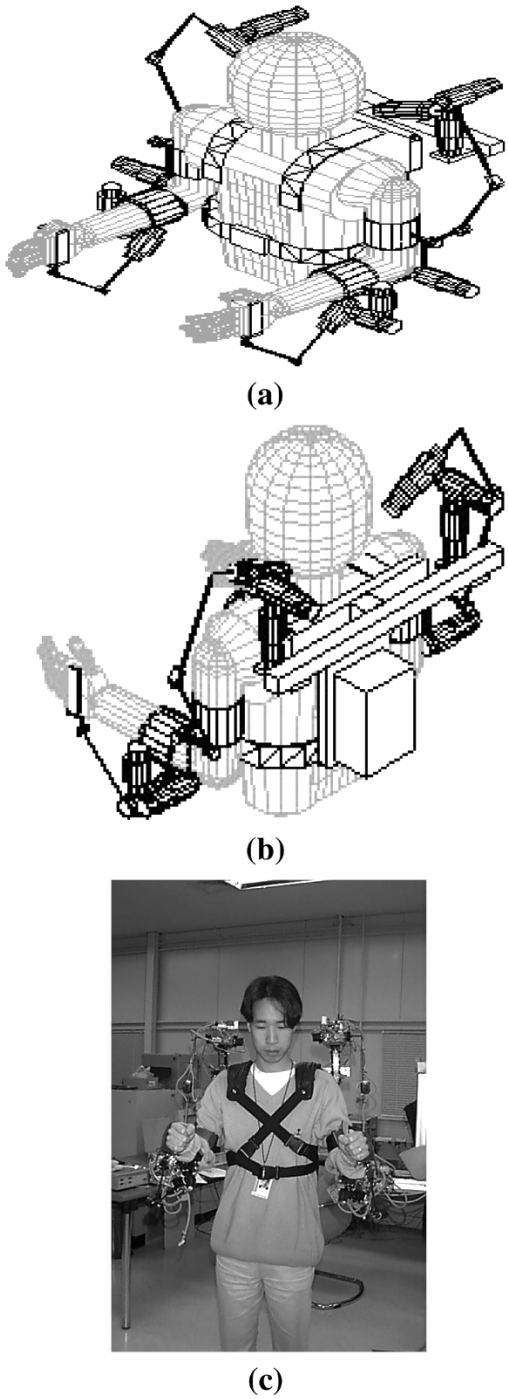

Fig. 2. Proposed exoskeleton-type masterarm. (a) The front, (b) the back, and (c) the photograph of the human operator on the masterarm.

6) Each joint should have an actuator for enabling force feedback.

Using a three-dimensional (3-D) graphic modeling/simulation package, various designs of the masterarm are tested as in Fig. 1. The final design is as follows:

1) Three measurable/controllable (active) joints +3 free (passive) joints for the shoulder.
2) One measurable/controllable (active) joint for the elbow.
3) Three measurable/controllable (active) joints +3 free (passive) joints for the wrist.

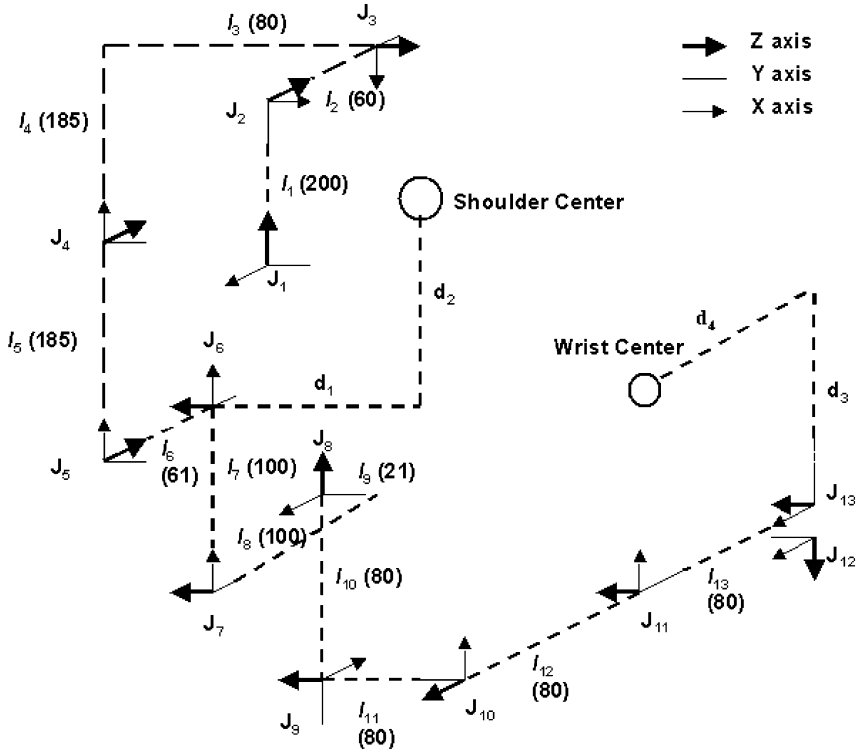

Fig. 3. Coordinates definition of the masterarm (left arm).

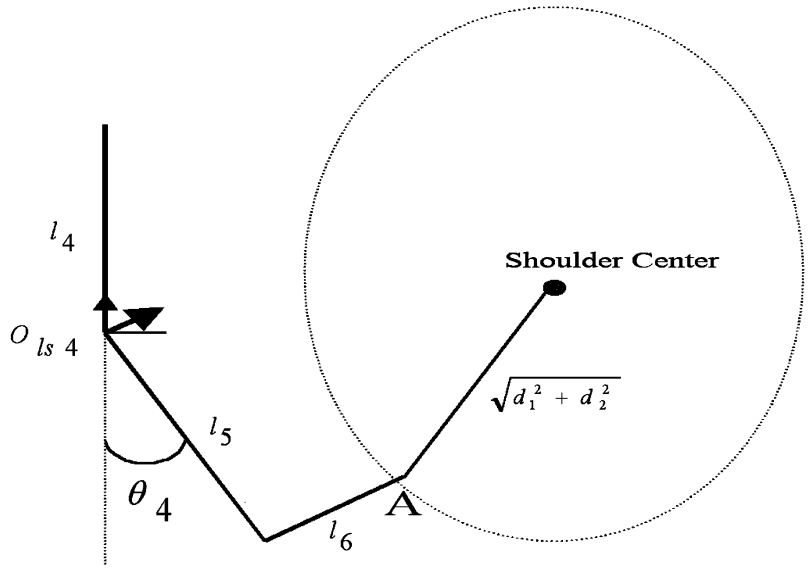

Fig. 4. Intersection point, A.

In Fig. 1, the upper arm is modeled with a ball-socket joint. By rotating the upper arm, the working range without collision is tested. Various combinations of the joint type, either revolute or prismatic, and link parameters are tested iteratively. Similar simulation is performed for the wrist part.

The final design of the masterarm is shown in Fig. 2. For the shoulder, the first three joints are active with encoders and electric brakes enabling force feedback. The other three are passive (free joints). Without measuring the free joints, the movement of the arm can be completely estimated, which is described in the following in detail. The weight of the masterarm is less than 3 kg.

The coordinates are defined as in Fig. 3. As previously mentioned, the first three joints are measurable, but the other three joints are not. Forward kinematics is defined as getting the initial location where the shoulder of the masterarm is fixed at the upper arm from the first three measurable joint angles. The following assumptions are used to complete the forward kinematics.

1) The locations of the shoulder and wrist center are known.
2) The location of the initial end point is known.
3) The shoulder joint is modeled as a ball-and-socket joint.

Along with these assumptions, only the kinematics of the shoulder part is described, since that of the wrist part is very

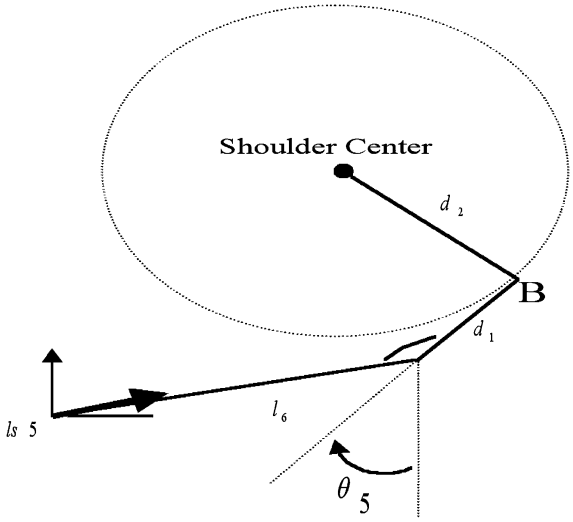

Fig. 5. Intersection point, B.

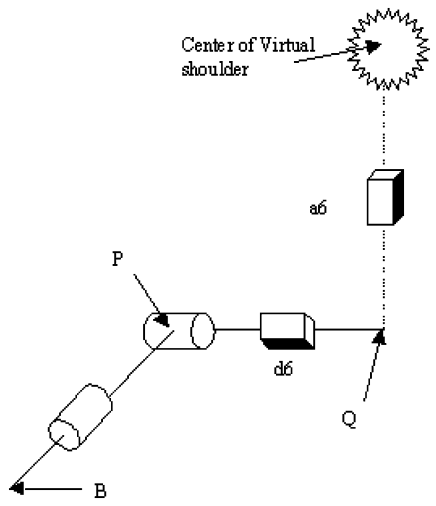

Fig. 6. Virtual shoulder for calibration.

similar. The calibration procedure to override these assumptions is required and described in Section III.

The first three angles are measurable and θ_4, θ_5, and θ_6 are unknown angles. First, θ_4 can be derived by finding the intersection point of two spheres as described in

$$x^2 + y^2 + z^2 = l_5^2 + l_6^2 \quad (1)$$

$$(x - P_{4x})^2 + (y - P_{4y})^2 + (z - P_{4z})^2 = d_1^2 + d_2^2 \quad (2)$$

where (P_{4x}, P_{4y}, P_{4z}) is the shoulder center point looked at from the origin of θ_4's coordinates O_{ls4}.

The intersection point A is located on the dotted circle as shown in Fig. 4. Let the point be (x_4, y_4, l_6), then (1) and (2) become

$$x_4^2 + y_4^2 = l_5^2 \quad (3)$$

$$(x_4 - P_{4x})^2 + (y_4 - P_{4y})^2 + (l_6 - P_{4z})^2 = d_1^2 + d_2^2. \quad (4)$$

From (3) and (4)

$$x_4 = \frac{\alpha P_{4x} \pm \sqrt{(\alpha P_{4x})^2 + \left(l_5^2 P_{4y}^2 - \alpha^2\right)\left(P_{4x}^2 + P_{4y}^2\right)}}{P_{4x}^2 + P_{4y}^2} \quad (5)$$

$$y_4 = \frac{\alpha - x_4 P_{4x}}{P_{4y}} \quad (6)$$

where

$$\alpha = \frac{P_{4x}^2 + P_{4y}^2 + l_5^2 - d_1^2 - d_2^2 + (l_6 - P_{4z})^2}{2}. \quad (7)$$

One of these solutions is not real, thus the valid solution is

$$\theta_4 = \tan^{-2}(y_4, x_4) - \pi \quad (8)$$

θ_5 is calculated similarly. The intersection point B is calculated by solving (9) and (10), and is shown in Fig. 5

$$x^2 + y^2 + z^2 = l_6^2 + d_1^2 \quad (9)$$

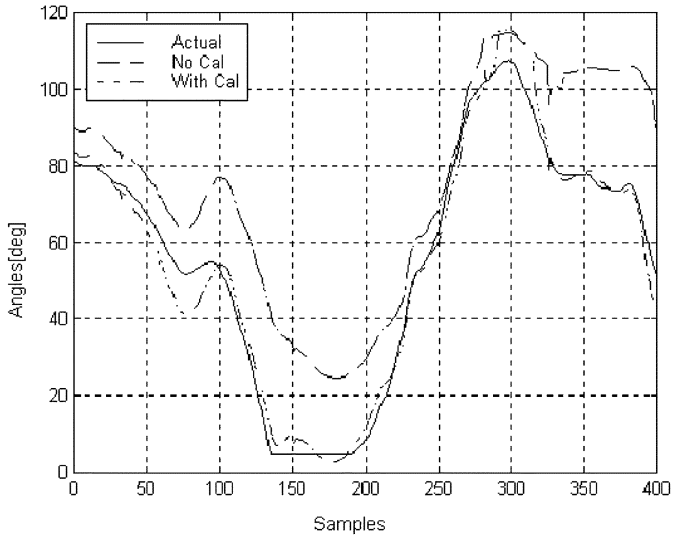

Fig. 7. Comparison of the measured, and calculated θ_4 with/without calibration.

$$(x - P_{5x})^2 + (y - P_{5y})^2 + (z - P_{5z})^2 = d_2^2. \quad (10)$$

By substituting $x_5, y_6,$ andl_6 into $x, y,$ and$z$, respectively

$$x_5 = \frac{\beta P_{5x} \pm \sqrt{(\beta P_{5x})^2 + \left(d_1^2 P_{5y}^2 - \beta^2\right)\left(P_{5x}^2 + P_{5y}^2\right)}}{P_{5x}^2 + P_{5y}^2} \quad (11)$$

$$y_5 = \frac{\beta - x_5 P_{5x}}{P_{5y}} \quad (12)$$

where

$$\beta = \frac{P_{5x}^2 + P_{5y}^2 + l_5^2 + d_1^2 - d_2^2 + (l_6 - P_{5z})^2}{2}. \quad (13)$$

Similar to θ_4, only one pair of solutions is valid

$$\theta_5 = \tan^{-2}(y_5, x_5) - \frac{\pi}{2}. \quad (14)$$

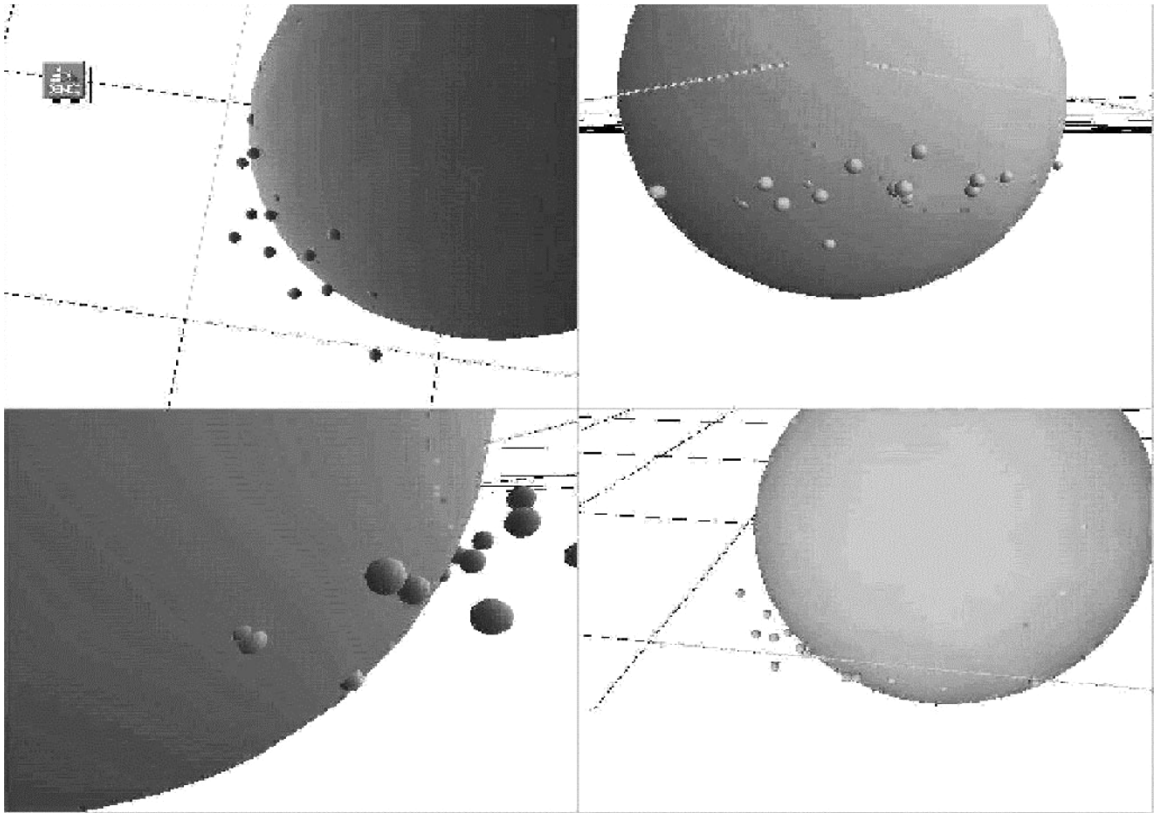

Fig. 8. Visualization of Calibration.

Since θ_4 and θ_5 are determined, θ_6 is unique as in

$$\theta_6 = \tan^{-2}(P_{6y}, P_{6x}) \tag{15}$$

where P_{6x} and P_{6y} are x and y coordinates of shoulder center point looked at from the origin of sixth rotational base.

III. Calibration

Forward kinematics is formulated geometrically in Section II with several assumptions. The masterarm has some parameters to be calibrated: the location of the shoulder center varies. The location of the initial end point is not always the same. The proposed masterarm uses encoders to measure θ_4 and θ_{11} (fourth joint of the upper arm and eleventh of the forearm) only for the purpose of the calibration. Once those parameters are estimated from calibration, it is not necessary to measure θ_4 anymore. Fig. 6 shows the concept of calibration: the center of the virtual shoulder is the shoulder center point. The location of P in Fig. 6 is always on the surface of a sphere centered at the virtual shoulder center. The location of the virtual shoulder center and the radius of the sphere are calculated using the least square method. In other words, various locations of P are gathered by freely moving the operator's arm from the measured θ_1, θ_2, θ_3, θ_4 and then the center and radius of the sphere are estimated. The location of the initial end point is calculated from the assigned posture of the operator. Fig. 7 shows the measured and calculated θ_4 before/after calibration, respectively. The calculated θ_4 after calibration (the dotted line) is matched well with the measured one (the solid line). The convergence of the least square method to find the center and radius is achieved only after five iterations with 45 data of P. Fig. 8 shows the results

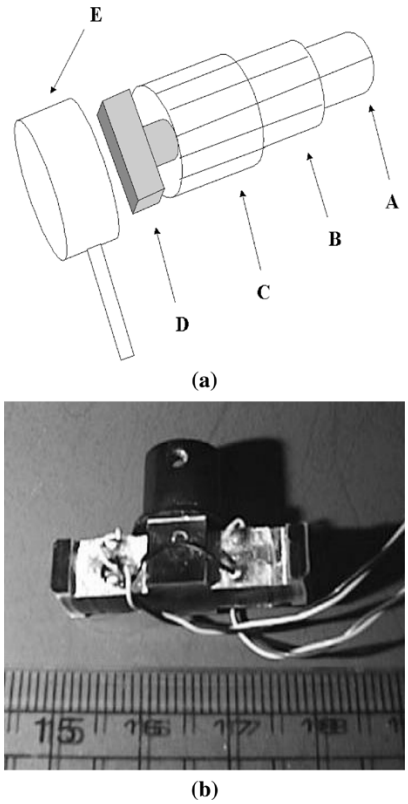

Fig. 9. (a) Active joint module and (b) torque sensor beam.

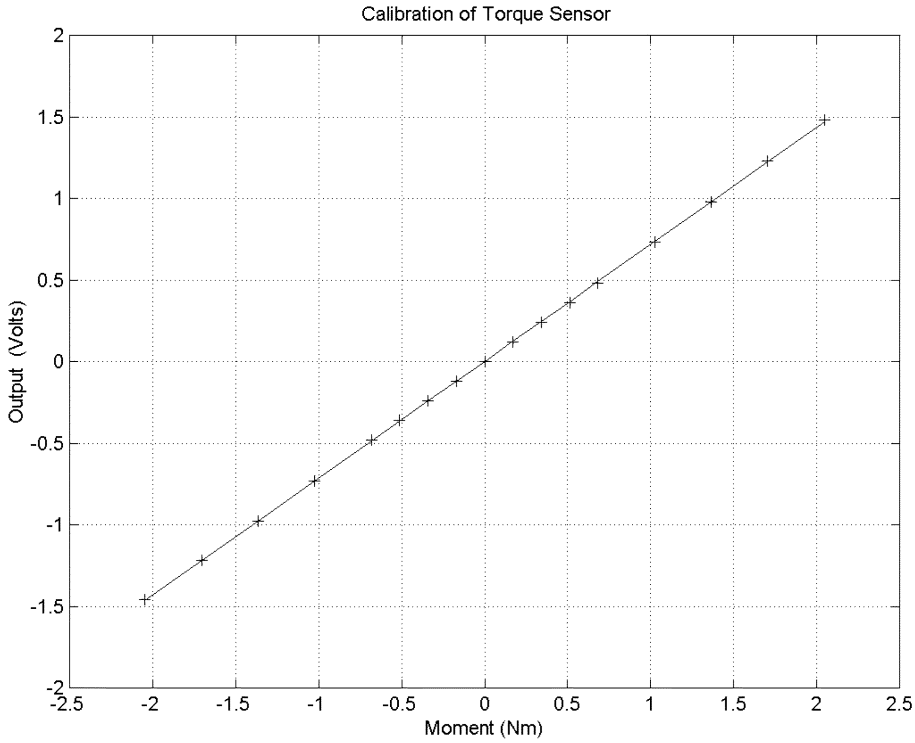

Fig. 10. Calibration result of the torque sensor beam (moment versus strain gauge voltage).

of the calibration. The small spheres are the measured P locations. The large sphere's radius and center location are estimated from calibration. The operator's shoulder joint is not exactly a ball-and-socket joint, and the joint location moves slightly as he moves his arm. When the operator stretches or lifts the upper arm, the shoulder joint also moves. Thus, the calculated virtual center/radius only produces the least amount of error, but not zero. This calibration algorithm is verified using the real ball-and-socket joint and, in this case, various sampled points of P are located exactly on a sphere after calibration. Similar calibration algorithms are derived for the wrist.

IV. Enabling Force Reflection

A. Design and Analysis

Most of the exoskeleton-type masterarms use the electric motors for force reflection. A torque sensor beam using the strain gauge is designed to allow an electric brake to be used as the actuator for force reflection [7]. It is necessary for the torque sensor beam to have the capabilities to detect both torque and its direction applied by the human operator. Each active (measurable/controllable) joint module is composed of an encoder (A), an electric brake (B), a gear head (C), a torque sensor beam (D), and a cover with link (E) as shown in Fig. 9. The encoder is used to measure the joint angle, and the electric brake is to constrain the joint motion with the applied torque. Once the electric brake is activated, the torque and its direction can be sensed from the torque sensor beam. In case the operator wants to move his arm toward the opposite direction of the applied torque, the electric brake is released so that he can move freely. Fig. 10 shows the calibration result of the torque sensor beam in terms of moment and the strain gauge output voltage. It shows linear characteristics

B. Distributed Controller Architecture

Most exoskeleton-type masterarms have encoders for measurement of the joint angles and actuators for force feedback. The actuators at each joint of the masterarm are to be controlled and the encoders are read for angle measurement. However, these simultaneous tasks make the control loop update rate low due to the sequential encoder reading (joint by joint) and actuator control. This may lead to some negative potentials: the wiring becomes quite bulky and induces electrical noise. The distributed controller architecture as shown in Fig. 11 is used for the proposed masterarm, instead of the centralized controller architecture: the controller of the proposed masterarm is composed of a host controller and satellite controllers. TMS320C31 (50 MHz) is used for the processor of host controller and PIC16C73 (20 MHz) for the satellite controller. The host controller performs the forward and the inverse kinematics calculation and data transmission to the slave robot controller. The satellite controller reads its joint angles as well as controls its actuator (brake). This distributed controller architecture reduces the control load of the host controller, thus, a higher data-update rate can be obtained. The host controller communicates with the satellite controllers via serial peripheral interface (SPI) protocol which requires only three wires and supports the daisy-chain connection: three signals (clock, serial data out, and serial data in) are required and each line is commonly shared by the satellite controllers (Fig. 12). The SPI network excels in implementation, maintenance, and expandability. Each satellite controller module is added to the SPI network with its unique identification number. (For more details, see [15] and [17].)

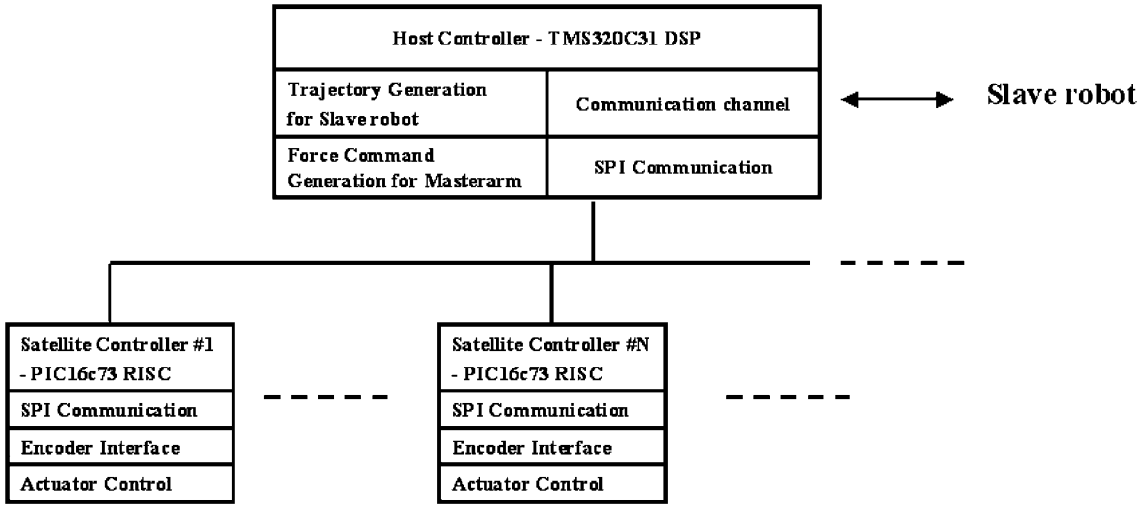

Fig. 11. Distributed controller architecture composed of the host controller and the satellite controllers. The host controller performs forward and inverse kinematics solution calculation and data transmission to the robot controller and satellite controller performs reading the corresponding joint angle, as well as controlling the actuators (electric brakes) to enable the force reflection.

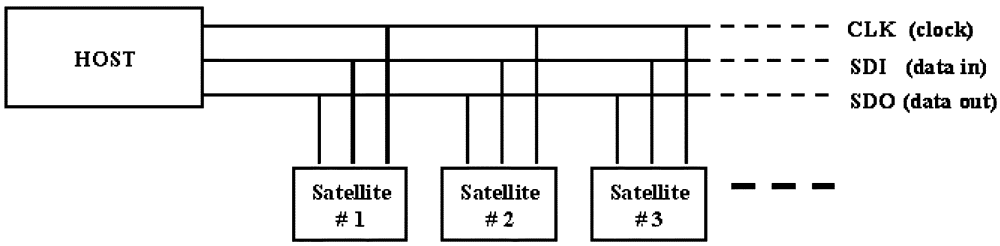

Fig. 12. SPI protocol linking the host controller and the satellite controllers.

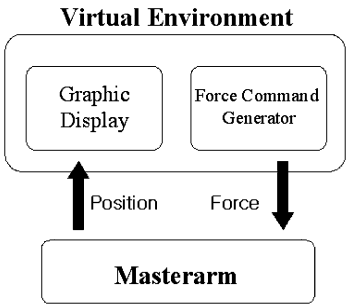

Fig. 13. Information flow of the VE with impedance causality: accepts position (velocity) and generates force.

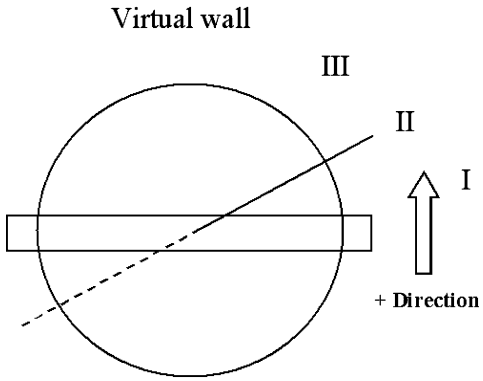

Fig. 14. Schematic diagram for experiment: (I) free motion regime, (II) contact regime, and (III) virtual wall regime.

C. Force Reflection

The proposed masterarm is used as a haptic device integrated with a computer-generated virtual environment (VE) for haptic interaction, as well as a motion commander integrated with a real robot for teleoperated interaction. Fig. 13 shows the information flow of the VE with impedance causality: accepts position (velocity) and generates force. Trajectory commands are generated as the human operator moves his arm. At the same time, the force information is fed back to the masterarm controller for force reflection. The force from the VE in contact is generated according to the torque sensed by the torque sensor beam (the force imposed to the robot is measured by the force/torque sensor attached at its wrists or the torque sensor at each joint). This force is converted to the force command to the masterarm to enable the force reflection. The torque applied to the human operator is based on the following equations

$$\overline{\tau}_i = J^T_{\text{master,i}}(\overline{\theta}_i)\overline{F}_{\text{slave,i}} \tag{16}$$

where

J	masterarm's Jacobian
$\overline{F}_{\text{slave,i}}$	$n \times 1$ slave robot's force/moment vector
$\overline{\tau}_i$	13×1 masterarm's joint torque vector

For simplicity, the first wrist joint θ_8 is integrated with the VE. In this test, the force exerted from the VE is calculated and reflected to the human operator. The experiment is composed of three parts as shown in Fig. 14: 1) free motion regime; 2) contact

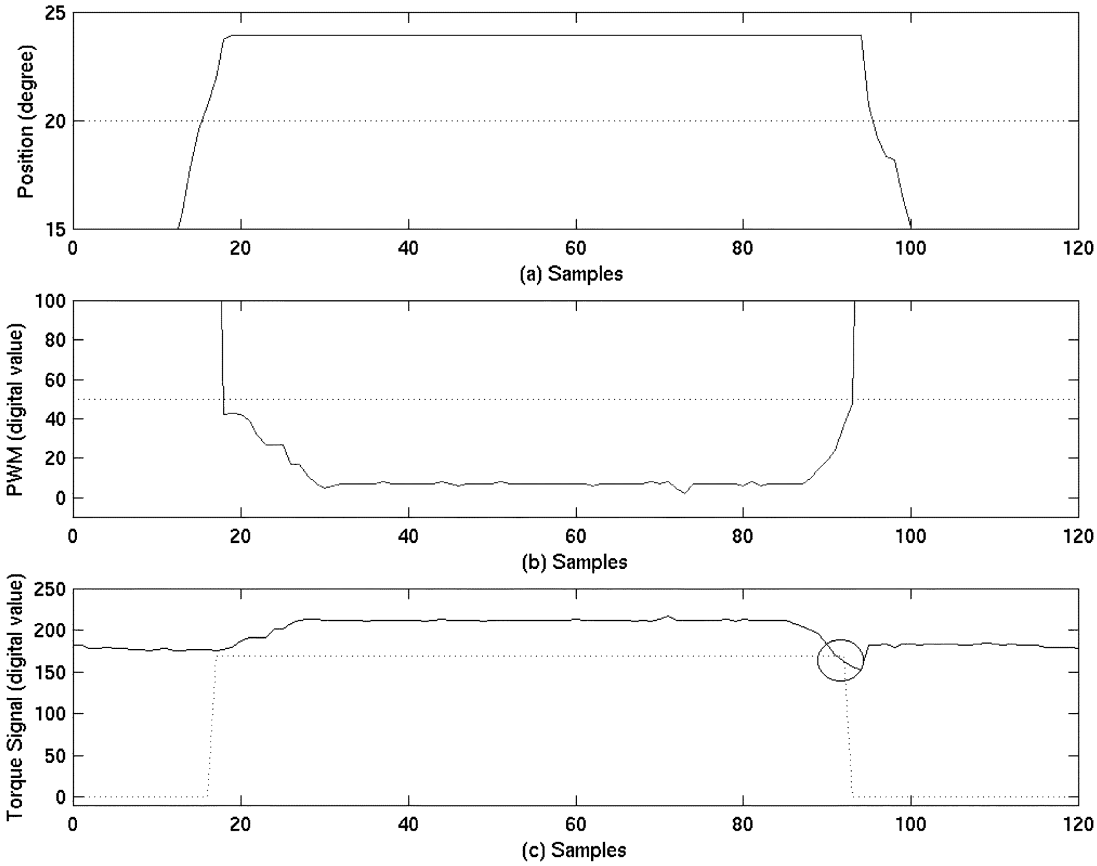

Fig. 15. Experiment result: (a) angle, (b) PWM, and (c) torque. The force applied to the human operator can be increased or decreased proportionally to the torque amount sensed by the torque sensor beam.

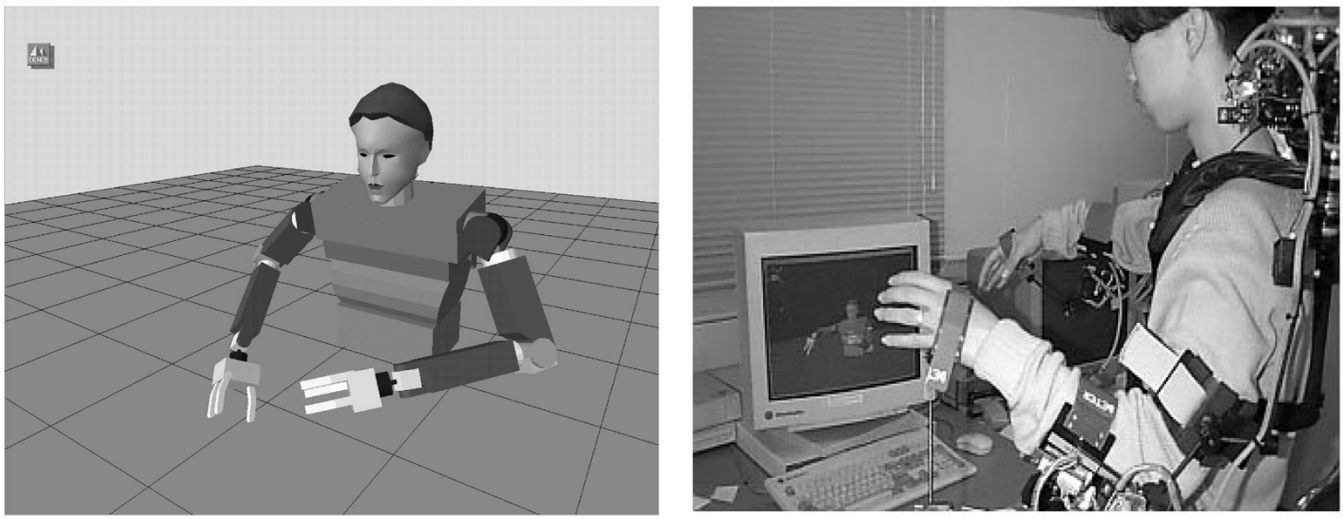

(a) **(b)**

Fig. 16. (a) Graphic model of a humanoid robot and (b) the haptic interaction with the human operator on the masterarm.

regime; and 3) virtual wall regime. The motion of the masterarm is restricted by the initial force sent from VE in the contact regime. As long as the contact is being kept, the force varies proportionally to the amount of the torque sensed by the torque sensor beam. When only the torque smaller than the initial offset is sensed (note that this is different from the initial force), the opposite direction is detected and, thus, the electric brake is released so that the operator can move freely. Fig. 15 shows the experimental results, which are 1) angle; 2) PWM command; and 3) torque signal, respectively. The contact regime was set at 20 °. Once contacted, the force is fed back to the masterarm to activate the electric brake at the same time. In Fig. 15(c), the initial offset (the dotted line) for detecting the opposite direction is set. During contact, we can see that the PWM command (the solid line) decreases (from 50 to 0, note that torque generated from the brake is inversely proportional to PWM command)

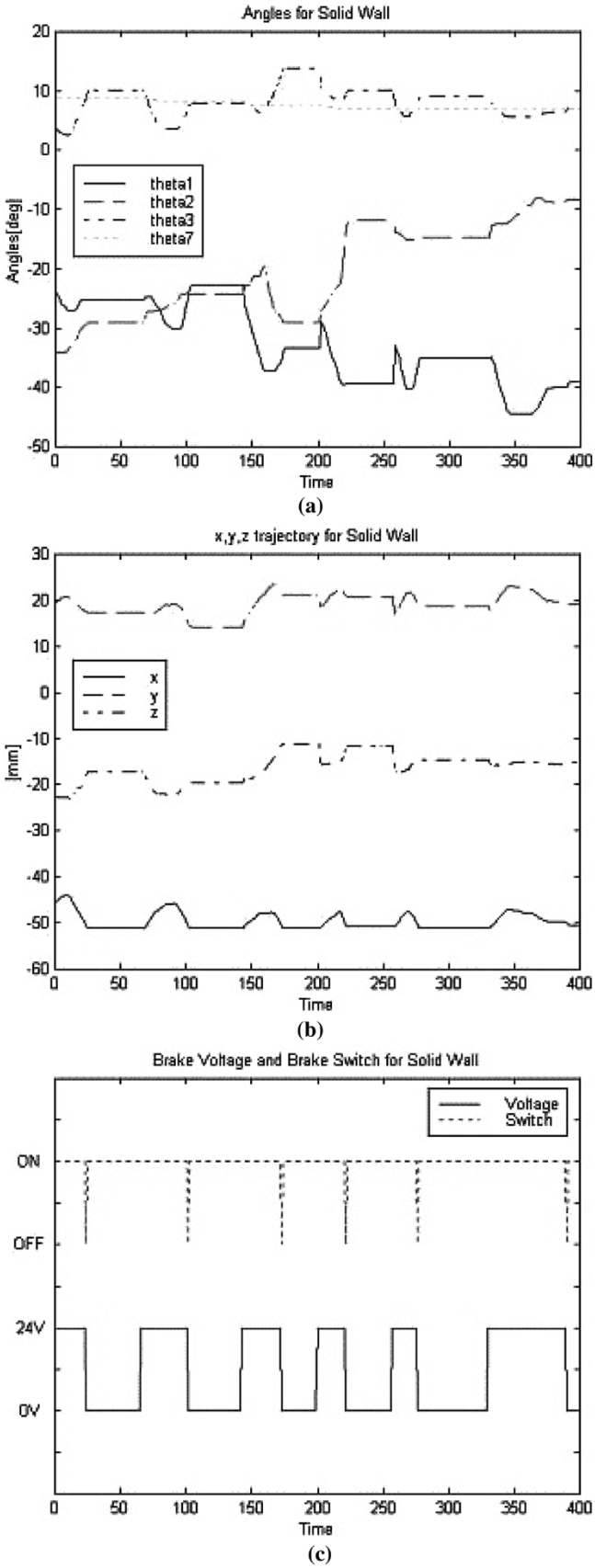

Fig. 17. (a) Hard contact with high stiffness (10 [KN/m]): angles, (b) each trajectory at end-point, and (c) brake voltage (PWM) and resetting the brake.

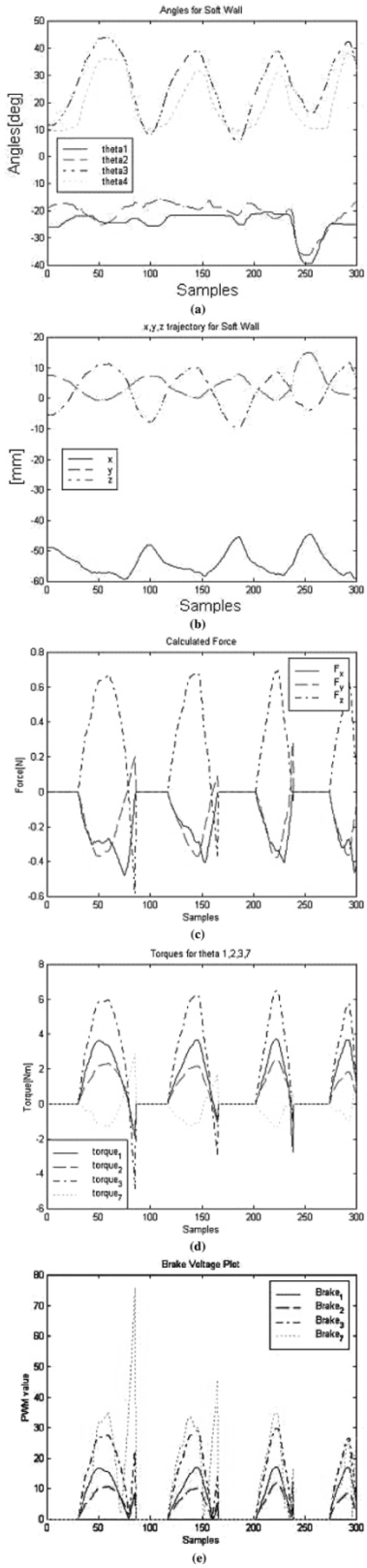

Fig. 18.(a) Soft contact with low stiffness (0.1 [N/m]): angles, (b) each trajectory at end-point, (c) forces reflected from the VE, (d) torques fed back to the human operator, and (e) increasing/decreasing PWM value to drive the brake torque proportionally to the torque sensed by the torque sensor beam.

and increases (from 0 to 50) proportionally to the torque amount sensed by the torque sensor beam: the difference between the sensed torque signal (the solid line) and the initial offset (the dotted line) is reflected to control the electric brake. When a

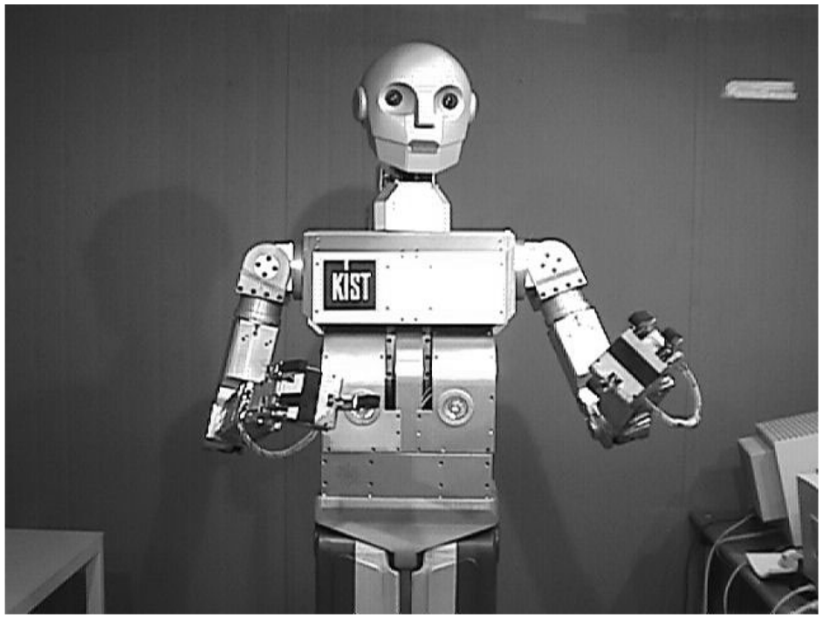

(a)

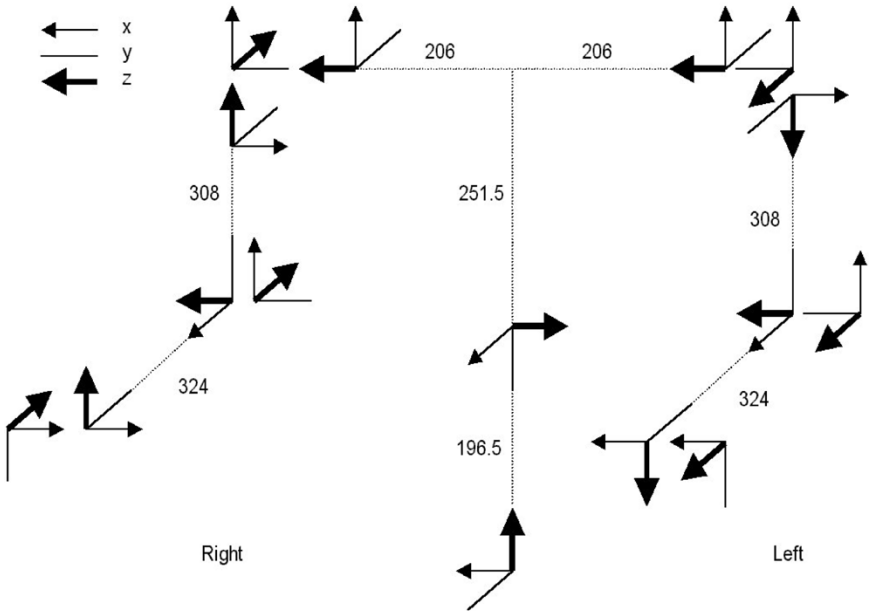

(b)

Fig. 19. Humanoid robot. (a) CENTUAR and (b) its coordinates definition (back view, in millimeters).

torque smaller than the initial offset (169) is sensed (the circle), the opposite direction (from II to I) is detected, and, thus, the electric brake is released (the PWM command becomes 255). This masterarm based on the torque sensor beam allows the operator to feel the same force during the contact without the numerical computation, which causes difficulties in determining visco-elastic parameters. With this proposed masterarm, we can freely design the force as the virtual robot interacts with the environment and the force reflection makes the operator feel as if he were moving toward an object and manipulate it. The proposed masterarm has been applied to various human–robot interactions, and some results are explored in Section V.

V. Human–Robot Interaction

A. Haptic Interaction With Virtual Environment

In this section, a haptic interaction with VE is explored using the proposed masterarm as a haptic device to allow the human operator to feel the forces virtually generated from the computer graphic contact model. Fig. 16 shows the graphic model of a humanoid robot and the haptic interaction with the operator

The force generated from the VE in contact is based on the following Hooke's law:

$$\overline{F}_{\mathrm{VE}} = k\overline{\Delta} \tag{17}$$

where, $\overline{F}_{\mathrm{VE}}$ is the reaction force, k is the stiffness, and $\overline{\Delta}$ is the amount of the interpenetration.

The torque applied to the human operator is obtained from (16). Haptic interactions with two different VE's are explored. The contact regime starts at $x = -500$ [mm], and the moment of roll-pitch-yaw direction is assumed to be zero for simplicity.

Hard Contact With High Stiffness: First, the masterarm is intergrated with VE with high stiffness (10 [KN/m]), which is a rigid wall. In this case, with such a rigid wall, the movements by the human operator (Δx, Δy, Δz) are very small, while the applied joint torques are very large. Therefore, in contact, the electric brakes should make the human operator hardly move. Also, it should allow the human operator to move freely in a free regime without contact by releasing the movement, especially when the human operator intends to move his arm toward the free regime in contact. Fig. 17(a) shows the joint trajectories of 1, 2, 3, and 7 ($\theta_1, \theta_2, \theta_3, \theta_7$) for this case. Fig. 17(b) shows each trajectory of x, y, z at end-point, and the movement is restricted to x axis. Fig. 17(c) shows how the electric brakes work as the human operator intends to move from contact to free regime. Fig. 17(c) shows how the electric brake is switched from contact to free regime by resetting the PWM value of the electric brake to zero to allow free motion. By detecting the torque and its direction, the electric brake allows the contact motion as well as the free motion by restricting or allowing the movement of the human operator.

Soft Contact With Low Stiffness: Second, the masterarm is intergrated with VE with low stiffness (0.1 [N/m]), which is a soft contact allowing deformation. Fig. 18(a) and (b) shows that the movements of the operator are relatively large compared to those of the hard contact with high stiffness. Fig. 18(c) and (d) shows the forces reflected from the VE and the torque fed back to the each joint of the masterarm, respectively. Fig. 18(e) shows the corresponding PWM value to drive the torque of the brake proportionally to the torque sensed by the torque sensor beam.

The haptic interaction with the proposed masterarm is tested and validated in two different cases. In soft contact with low stiffness, the force reflected is proportional to the amount of the deformation (equivalent to the amount of the torque sensed by the torque sensor beam) during contact allowing soft feeling. On the other hand, in hard contact with high stiffness, the force is realized as if the human operator feels the force contacting with a rigid wall by providing each joint with large torque (thus sending a large force command for force reflection).

B. Teleoperated Interaction

KIST Humanoid Robot: The proposed masterarm is designed not for a specific type of a slave robot. It can be integrated with a slave robot with adequate Kinematic transformation that matches the posture of the slave robot to that of the human operator. In this section, Kinematic transformation is described for integration with the humanoid robot CENTAUR. The photo and the coordinates definition of CENTAUR are shown in Fig. 19. CENTAUR has 3, 1, and 3 degrees of freedom (D.O.F.) in each shoulder, elbow, and wrist, respectively. It has also 2 D.O.F. on the neck and waist. Its kinematics structure is similar to that of a human. From the forward kinematics of the proposed masterarm in Section II, the followings are also determined for Kinematic transformation to the humanoid robot.

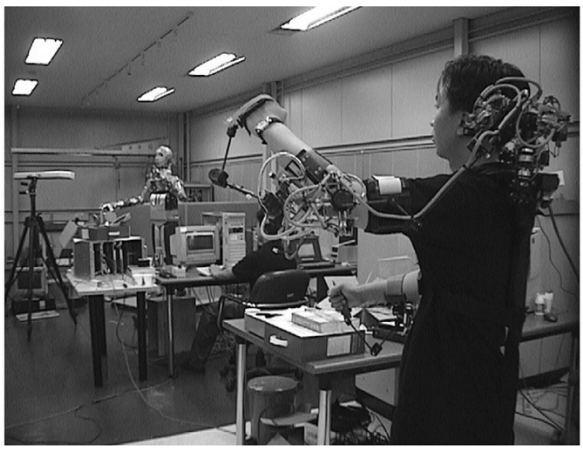

(a)

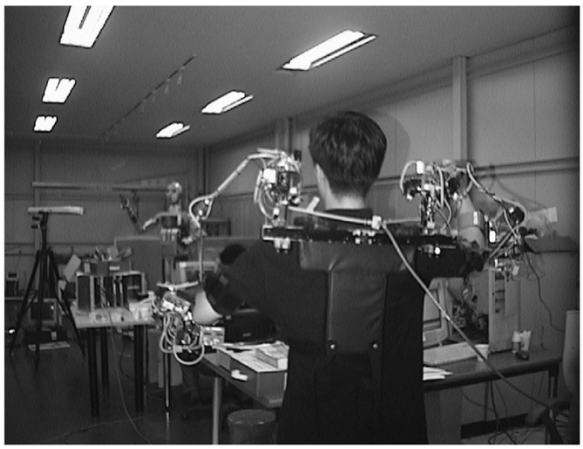

(b)

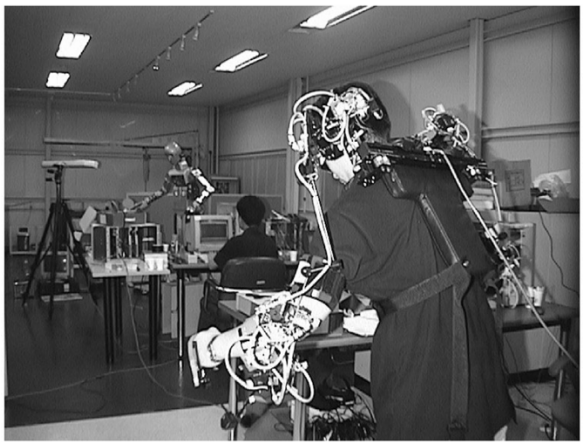

(c)

Fig. 20. Posture/motion test: (a) left arm posture, (b) right arm posture, and (c) upper body posture.

A	operator's shoulder center point
B	operator's elbow center point
C	operator's wrist center point
θ_{me}	masterarm's elbow joint angle
Rot	operator's wrist orientation matrix (3 by 3)

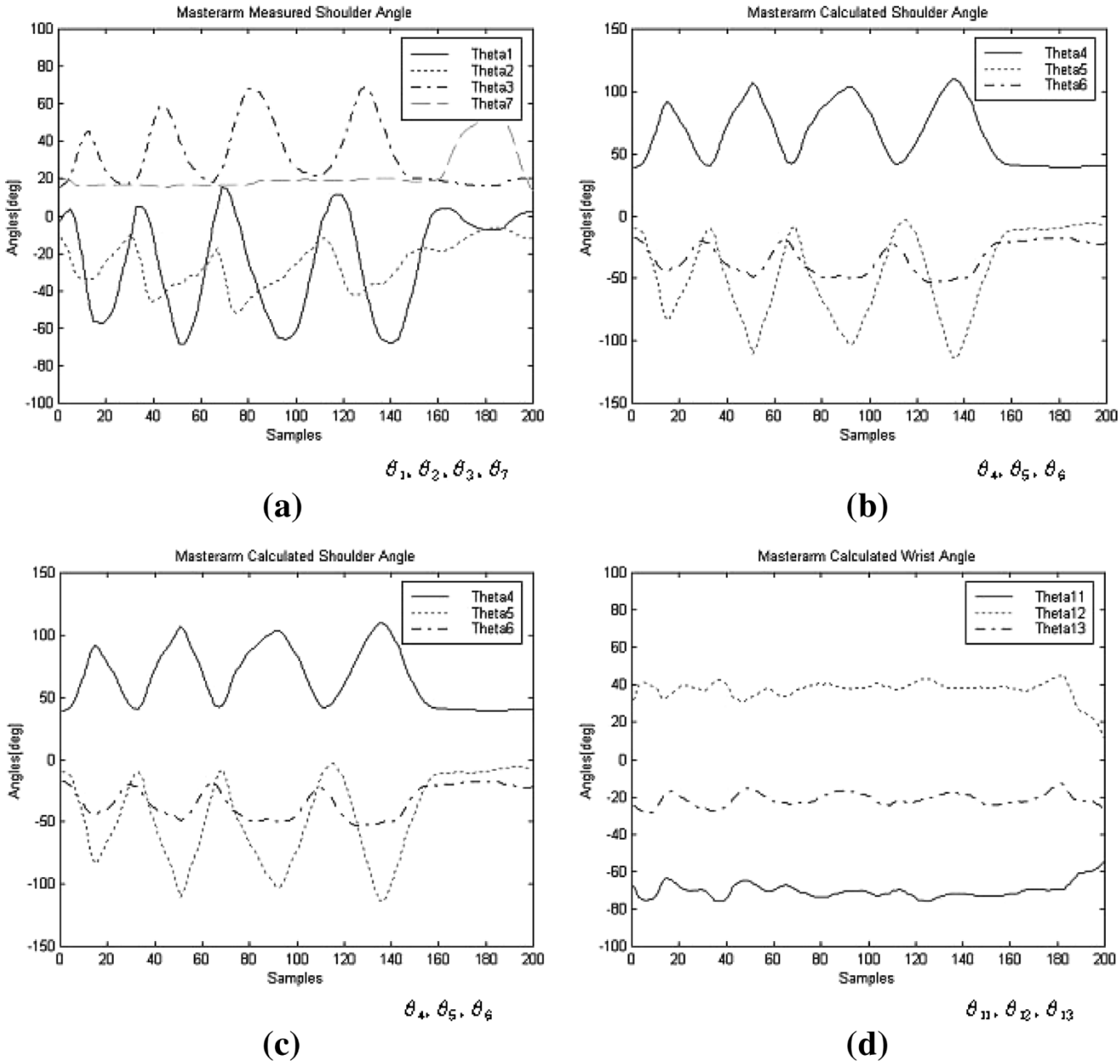

Fig. 21. Joint trajectories of the masterarm during the posture/motion test: (a) the measured and (b) calculated joints of the upper arm, and (c) the measured and (d) calculated joints of the forearm.

The Kinematic transformation of the proposed masterarm to CENTAUR is achieved as following:

1) CENTAUR's upper arm is calculated with A, B, and C.
2) Elbow angle is matched to $\theta_{\rm me}$
3) Wrist angle is calculated from the comparison between matrix *Rot* and rotation matrix of CENTAUR's wrist.

The transformation is described as follows. Considering the right arm only, and defining angles as $\theta_1, \theta_2, \ldots, \theta_7$ from the shoulder to the wrist

$$\theta_1 = \tan^{-2}(\overrightarrow{AB_{1y}}, \overrightarrow{AB_{1x}}) + \pi \tag{18}$$

$$\theta_2 = \tan^{-2}(\overrightarrow{AB_{2y}}, \overrightarrow{AB_{2x}}) + \pi \tag{19}$$

$$\theta_3 = \tan^{-2}(\overrightarrow{BC_{3y}}, \overrightarrow{BC_{3x}}) + \frac{\pi}{2} \tag{20}$$

where $\overrightarrow{XY_n}$ means vector XY viewing at the nth coornate system.

For the elbow and the wrist

$$\theta_4 = -\theta_{\rm me} \tag{21}$$

$$\theta_6 = \tan^{-2}\left(\sqrt{r_{13}^2 + r_{23}^2}, r_{33}\right) \tag{22}$$

$$\theta_5 = \tan^{-2}\left(\frac{r_{13}}{\sin\theta_6}, -\frac{r_{23}}{\sin\theta_6}\right) \tag{23}$$

$$\theta_7 = \tan^{-2}\left(-\frac{r_{32}}{\sin\theta_6}, \frac{r_{31}}{\sin\theta_6}\right) \tag{24}$$

where $r_{\rm mn}$ means element in the mth row and the nth column in *Rot* matrix. (For more details, see [18] and [19].)

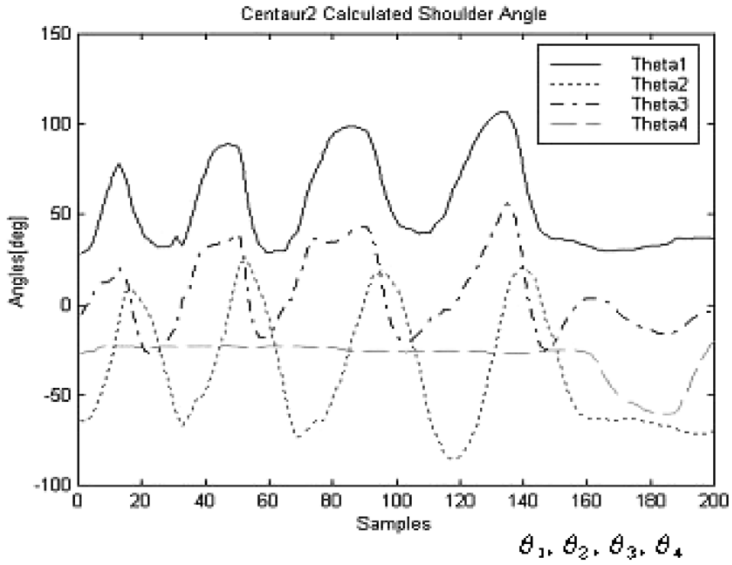

(a)

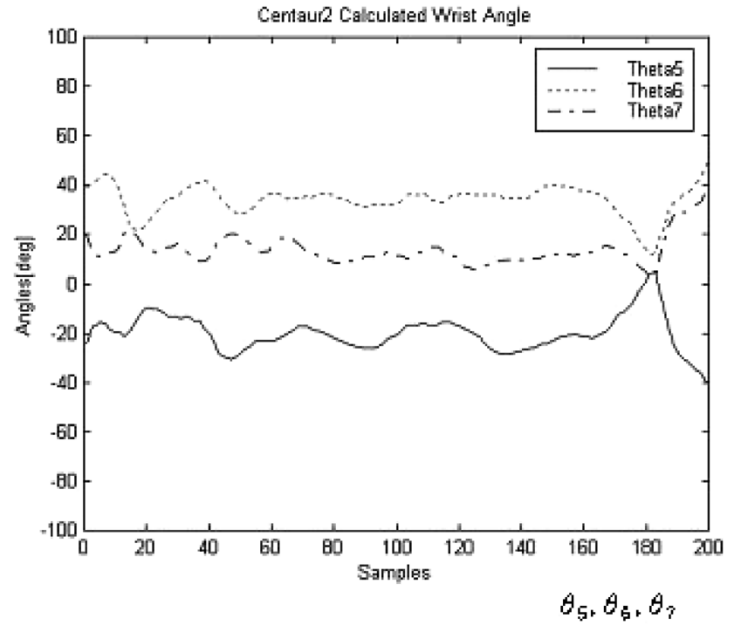

(b)

Fig. 22. Joint trajectories of the robot sent from the masterarm during the posture/motion test. (a) the upper arm joints and (b) the forearm joints. Those joints are all calculated by the joint coordinates transformation and sent to the robot to follow the movement of the human operator on the masterarm.

Pick-and-Place Task: Kinematics described above show how to integrate the masterarm with any slave robot. A teleoperated interaction is performed using the masterarm as a motion commander. Some snapshots of the experiments are given in Fig. 20, showing the robot follows the movement of the operator. Figs. 21 and 22 show all the joint trajectories of the masterarm and the robot measured and calculated during the experiment. After this validation, on the motion following, a human–robot integration through the teleoperated interaction is conducted. The given task is a complex sequential pick-and-place task. The robot picks up a rose and a vase using each arm/hand separately, puts the rose into a vase, and places the vase on the table commanded by the operator's movement. Fig. 23(a) shows the schematic diagram of the teleoperated interaction with the humanoid robot. Two mastergloves and a Fastrak sensor (motion-capturing sensor) are added to the overall system, as shown in the figure to generate the motions of the CENTAUR's waist, neck, and hands (fingers). The mastergloves are used for the robot fingers' grasping motion, only without force feedbacks, because robot fingers do not have force-sensing capability. The VME bus based on multicontrollers is used with the VxWorks real-time operating system for controlling the robot. Fig. 23(b) and (e) shows some snapshots of consecutive teleoperated interaction (which lasted for about 2.5 min) using the proposed masterarm.

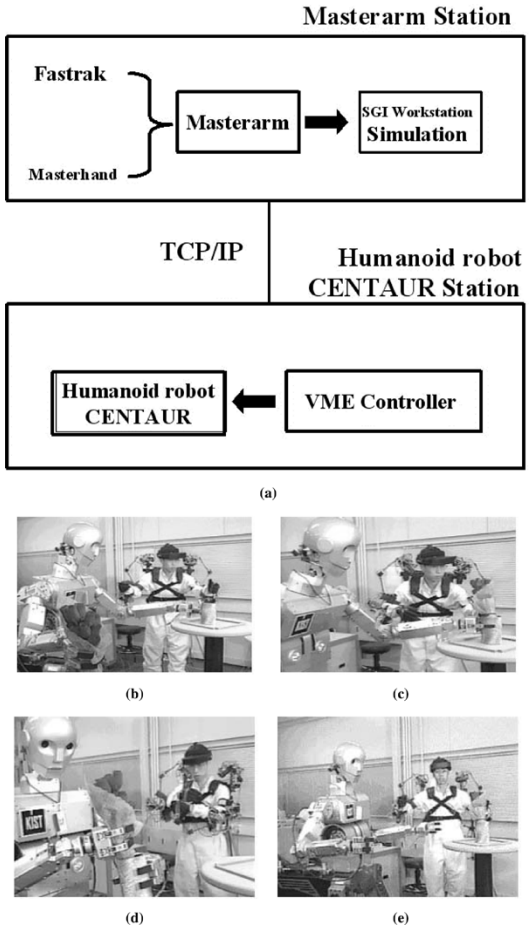

Fig. 23. Teleoperated Interaction. (a) Schematic diagram, (b) the robot approaching the table, (c) picking up the vase, (d) putting the rose into the vase, and (e) placing the vase on the table.

VI. Conclusion

Human–robot interactions are explored in this paper with a new exoskeleton-type masterarm, in which electric brakes combined with the torque sensor beam as actuators for force reflection. In hard contact, the electric brake with the torque sensor beam can detect the torque and its direction so that it allows the free motion or constrained motion. The results show how the electric brake is switched from contact to free regime to allow free motion of the human operator, especially when the human operator intends to move toward the free regime in contact. In soft contact, the force applied to a human operator is proportional to the torque amount sensed by the torque sensor beam, and the human operator thus can feel the contact force proportional to the amount of the deformation during contact. The masterarm is integrated with the humanoid robot, CENTAUR.

References

[1] T. B. Sheridan, *Telerobotics, Automation and Human Supervisory Control*. Cambridge, MA: MIT Press, 1992.
[2] R. Goertz, "Manipulator systems development at ANL," presented at the 12th Conf. Remote Syst. Technol., vol. 12, 1964.
[3] G. C. Burdea, *Force and Touch Feedback for Virtual Reality*. New York: Wiley, 1996.
[4] B. Hannaford and S. Venema, "Kinesthetic display for remote and virtual environment," in *Virtual Environment and Advanced Interface Design*, W. Barfield and T. A. Furness, Eds. Oxford, UK: Oxford Univ. Press, 1995, pp. 415–436.
[5] J. M. Hollerbach, "Some current issues in haptics research," in *Proc. IEEE Int. Conf. Robot. Automation*, vol. 1, San Francisco, CA, 2000, pp. 757–762.
[6] J. W. Hill, J. F. Jensen, P. S. Green, and A. S. Shah, "Two-Handled telepresence surgery demonstration systems," presented at the ANS 6th Annu. Topical Meeting Robot. Remote Syst., 1995.
[7] M. Bergamasco, B. Allotta, L. Bosio, L. Ferretti, G. Parrini, G. M. Prisco, F. Salesdo, and G. Sartini, "An arm exoskeleton system for teleoperation and virtual environments applications," in *Proc. IEEE Int. Conf. Robot. Automation*, vol. 2, San Diego, CA, 1994, pp. 1449–1454.
[8] S. C. Jacobsen, F. M. Smith, D. K. Backman, and E. K. Iversen, "High performance, high dexterity, force reflective teleoperator," in *Proc. 38th Conf. Remote Syst. Technol.*, Washington, DC, 1990, pp. 180–185.
[9] M. Bouzit, G. Burdea, G. Popescu, and R. Boian, "The rutgers master II-new design force-feedback glove," *IEEE/ASME Trans. Mechatron.*, vol. 7, pp. 256–263, 2002.
[10] The Cyberglove/Cybergrasp. Immersion Corp.. [Online]. Available: http://www.immersion.com/
[11] The Logitech WingMan. [Online]. Available: http://www.logitech.com/
[12] The PHANToM. SensAble Technology Inc.. [Online]. Available: http://www.sensable.com/)
[13] S. Lee, S. Park, M. Kim, and C.-W. Lee, "Design of a force reflecting master arm and master hand using pneumatic actuators," in *Proc. IEEE Int. Conf. Robot. Automation*, vol. 3, Leuven, Belgium, 1998, pp. 2574–2579.
[14] S. Lee, D. Choi, M. Kim, C.-W. Lee, and J.-B. Song, "An unified approach to teleoperation : Human and robot integration," in *Proc. IEEE/RSJ Int. Conf. Intell. Robots Syst.*, vol. 1, Victoria, Canada, 1998, pp. 261–266.
[15] S. Lee, J. Lee, D. Choi, M. Kim, and C.-W. Lee, "The distributed controller architecture for a masterarm and its application to teleoperation with force feedback," in *IEEE Int. Conf. on Robotics and Automation*, vol. 1, Detroit, MI, 1999, pp. 213–218.
[16] Y. S. Kim, S. Lee, C. Cho, M. Kim, and C.-W. Lee, "A new exoskeleton-type masterarm with force reflection based on the torque sensor beam," in *IEEE Int. Conf. on Robotics and Automation*, vol. 3, Seoul, Korea, 2001, pp. 2628–2633.
[17] S. Lee, J. Lee, W. Chung, M. Kim, C.-W. Lee, and M. Park, "A new exoskeleton-type masterarm with force reflection: Controller and integration," in *Proc. IEEE/RSJ Int. Conf. Intell. Robots Syst.*, vol. 3, 1999, pp. 1438–1443.
[18] S. Lee, J. Lee, M. Kim, and C.-W. Lee, "A new master-arm for man-machine interface," in *Proc. IEEE Int. Conf. Syst., Man, Cybern.*, vol. 4, 1999, pp. 1038–1043.
[19] M. Kim, S. Kang, S. Lee, W. Chung, K. Cho, and C.-W. Lee, "Development of a humanoid robot CENTAUR-design, human interface, planning and control of its upper-body," in *Proc. IEEE Int. Conf. Syst., Man, Cybern.*, vol. 4, 1999, pp. 948–953.

Yoon Sang Kim (M'04) received the B.S., M.S., and Ph.D. degrees in electrical engineering, from Sungkyunkwan University, Suwon, Korea, in 1993, 1995, and 1999, respectively.

He was a Member of the Post-Doctoral Research Staff of the Humanoid Robotics Research Center, Korea Institute of Science and Technology (KIST), Seoul, Korea. He was also a Faculty Research Associate in the Department of Electrical Engineering, University of Washington, Seattle. Since October 2003, he has been a member of Senior Research Staff with the Interaction Laboratory, Samsung Advanced Institute of Technology (SAIT), Suwon, Korea. His current research interests include haptic technology and device-based interactive application.

Dr. Kim was awarded Korea Science and Engineering Foundation (KOSEF) Overseas Postdoctoral Fellow in 2000.

Jangwook Lee received the B.S. degree in control and instrumentation engineering from Sungkyunkwan University, Suwon, Korea, in 1997 and the M.S. degree in electric and computer engineering from Yonsei University, Seoul, Korea, in 1999.

From 2000 to 2002, he was a Research Scientist at the Samsung SDI Corporate Research and Development Center. Since 2002, he has been a Software Specialist with Telecom Billing System, SK C&C, Seoul, Korea. His currents interests are teleoperation and internet-based home appliances.

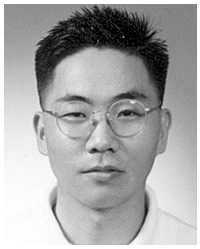

Sooyong Lee (S'94–M'04) received the B.S. and M.S. degrees in mechanical engineering from Seoul National University, Seoul, Korea, in 1989, and 1991, respectively, and the Ph.D. degree from Massachusetts Institute of Technology, Cambridge, MA, in 1996.

He was a Senior Research Scientist at Korea Institute of Science and Technology (KIST), Seoul, Korea. He was also an Assistant Professor in the Department of Mechanical Engineering, Texas A&M University, College Station. He joined Hongik University, Seoul, Korea, in 2003 and is currently an Assistant Professor in the Mechanical and System Design Engineering Department. His current research interests include mobile robot localization and navigation and active sensing.

Prof. Lee received the National Science Foundation Career Award in 2003 and the Kayamori Best Paper Award at the 1997 IEEE International Conference on Robotics and Automation.

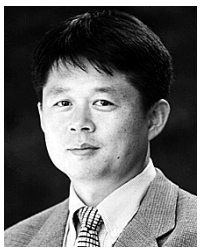

Munsang Kim (M'91) received the B.S. and M.S. degrees in mechanical engineering from the Seoul National University, Seoul, Korea, in 1980 and 1982, respectively, and the Dr.-Ing. degree in robotics from the Technical University of Berlin, Berlin, Germany, in 1987.

Since 1987, he has been a Research Scientist at the Korea Institute of Science of Korea, Seoul. He has led the Advanced Robotics Research Center since 2000 and became the Director of the "Intelligent Robot–The Frontier 21 Program" in October 2003. His current research interests are the design and control of novel mobile manipulation systems, haptic device design and control, and sensor application to intelligent robots.